Graphitic Carbon Nitride Nanosheet as an Excellent Compound for the Adsorption of Calcium and Magnesium Ions: Theoretical and Experimental Studies

Chegeni, Mahdieh**+; Enjedani, Mehrnosh

Department of Chemistry, Ayatollah Boroujerdi University, Boroujerd, I.R. IRAN

ABSTRACT: *In this work, the removal of calcium (Ca^{2+}) and magnesium (Mg^{2+}) ions was studied using graphitic carbon nitride (g-C_3N_4) nanosheet as an adsorbent from aqueous solutions. In experimental studies, the effects of various adsorption parameters were investigated by batch method culture including pH, initial Ca^{2+} and Mg^{2+} concentrations, temperature, time, and adsorbent mass. The best results were obtained at pH=8.50, 0.05 g of g-C_3N_4, 90 min, 10 ppm of ion concentration, 23.80 mg/g of maximum adsorption capacity for Ca^{2+}, and pH=9, 0.05 g of g-C_3N_4, 60 min, 15 ppm of ion concentration, 40.00 mg/g maximum adsorption capacity for Mg^{2+} ion. The adsorption of calcium and magnesium ions obeyed the Langmuir model on the adsorbent. In a theoretical study, g-C_3N_4 nanosheet as an interesting material was studied by first-principle calculation using the Quantum Espresso package. The Ca^{2+} and Mg^{2+} ions were located at different positions on g-C_3N_4 nanosheet to obtain a stable configuration. The E_{ads}, HOMO, LUMO, E_g, band structure, DOS, and PDOS plots were investigated at a stable configuration of g-C_3N_4 nanosheet. The adsorption energy (E_{ads}) was calculated -15.55 and -26.24 eV for Ca^{2+} and Mg^{2+} ions, respectively. Further, the results indicated that Mg^{2+} can be located at the center of the porous g-C_3N_4 nanosheet, and the adsorption of Mg^{2+} on the surface of g-C_3N_4 nanosheet was stronger than that of Ca^{2+} ion. Theoretical and experimental data confirmed each other's findings. The adsorption of Ca^{2+} and Mg^{2+} ions was shown to be simple, high-yield, eco-friendly, and economical performance from aqueous solutions using g-C_3N_4 nanosheet.*

KEYWORDS: *Graphitic carbon nitride nanosheet; Adsorption; Calcium; Magnesium; DFT.*

INTRODUCTION

The study of ions interactions on materials is essential for designing novel compounds. Researchers have attempted to discover sensing platforms for ions indication [1-2]. The evaluation of ionic interaction with surfaces is an interesting subject, because of its application in chemical and electronic sensors. Among various ions, a few articles were reported regarding calcium (Ca^{2+}) and magnesium (Mg^{2+}) ions' interactions with compound surfaces.

** To whom correspondence should be addressed.*
+ E-mail: mahdieh.chegeni@abru.ac.ir
1021-9986/2022/5/1512-1527 10/$/6.01

The Ca^{2+} ion is an essential mineral in the human body [3]. Further, high amounts of magnesium ions can lead to a fall in blood pressure, muscle weakness, and impaired breathing [4, 5]. Furthermore, the cleaning yield of detergents might be decreased, due to the reaction of Ca^{2+} and Mg^{2+} ions with soap anions. In addition, the application of these ions in electronic objectives is an important issue in surface chemistry. Therefore, the construction of new compounds is a valuable subject, which can be employed as a sensor or adsorbent for Ca^{2+} and Mg^{2+} ions.

Among water softening methods, the electrochemical procedure [6], enzyme-catalyzed technique [7], nanofiltration [8], ultra-filtration [9], and pulsed spark discharge [10] have been used extensively. Some of these methods are expensive, require post-treatment, excessive use of organic solvents, and can be produced large volumes of sludge. The undesired reaction between the analyte and adsorbent can be considered a disadvantage of electrochemical procedure, which can be changed conductivity [11]. Further, the process of adsorption has offered several advantages such as high yield, simplicity, lack of by-product, and ease of operation [12], but the slow rate of some adsorbents has proposed the importance of designing a new adsorbent.

Several adsorbents based on carbon were used including fullerene [12], carbon nanotube [13], carbon activated [14], and Bagasse [15]. In carbon structure compounds, Liu and Cohen predicated graphene-like carbon nitride [16]. Graphitic carbon nitride (g-C_3N_4) can be synthesized using a simple strategy from melamine, cyanamide, dicyandiamide, guanidine, or hydrochloride urea as starting materials [17]. The properties of g-C_3N_4 have raised from its special electronic structure, which exhibits fantastic properties such as chemical and thermal stability, low cost, biocompatibility, and stability in water and acid-basic solvents.

2D carbon nitride can be employed in many fields such as full cells [18], electrocatalysts [19], adsorbents [20], photocatalysts [21], and H_2 generation from water splitting [22] with the potential for the formation of various composites [17, 23-25]. The g-C_3N_4-based composites have exhibited photocatalytic performance such as ZnO/g-C_3N_4 [23], CdS/g-C_3N_4 [24], AgBr/g-C_3N_4 [25], and NiFe-LDH/g-C_3N_4 [26]. In theoretical studies, graphitic carbon nitride has been studied for the adsorption of aspirin [27], and CO_2 [28]. In experimental performance, g-C_3N_4 nanosheet has been used as a chemosensor for Cu^{2+} [29] and pb^{2+} [30], because it can be shown with high surface area and active sites.

To the best of our knowledge, a few theoretical and experimental studies have been reported about the adsorption of Ca^{2+} and Mg^{2+} ions. In 2013, the adsorption of Ca^{2+} and Mg^{2+} ions on carbon nitride nanotube was discussed via a theoretical study [10]. In another research, the properties of Ca^{2+} and Mg^{2+} ions adsorbed on {1014} calcite surface were investigated [31]. Also, the experimental adsorption of these ions was considered by marine cyanobacterium (*Gloeocapsa sp*.) [32] and *Pistacia Vera* shell [33]. It is noticeable that some studies have provided only theoretical or experimental results.

The choice of Ca^{2+} and Mg^{2+} ions were selected for two reasons:

1) the importance of selected ions in the quality of water.

2) the application of Ca^{2+} and Mg^{2+} ions for designing new nanostructured materials for field emission or sensor applications. In addition, g-C_3N_4 nanosheet can be worked as an adsorbent or electronic sensor, but reported compounds have shown one of these applications.

In this regard, we aimed to present the experimental and theoretical studies for the adsorption of calcium and magnesium ions on graphitic carbon nitride nanosheet (Fig. 1). First, the effect of different parameters were investigated for adsorption by bath culture, then the theoretical evaluation was carried out *via* the first principle study for bare and modified g-C_3N_4 nanosheets using Ca^{2+} and Mg^{2+} ions. Various parameters were calculated including E_g (Gap Energy), HOMO (Highest Occupied Molecular Orbital), and LUMO (Lowest Unoccupied Molecular Orbital) energies, the band structure, DOS (Density of States), and PDOS (Partial Density of States) plots, as well as E_{ads} (Adsorption Energy). Finally, this study demonstrates the benefit of g-C_3N_4 nanosheet as an adsorbent or sensor for Ca^{2+} and Mg^{2+} ions.

EXPERIMENTAL SECTION

Materials and instruments

Melamine, calcium chloride ($CaCl_2$), magnesium chloride ($MgCl_2$), sodium hydroxide (NaOH), and hydrochloric acid (HCl) were purchased from Merck and Fluka companies. Fourier Transform Infra-Red (FT-IR) spectroscopy spectra and Field Emission Scanning Electron Microscopy (FE-SEM) images were recorded

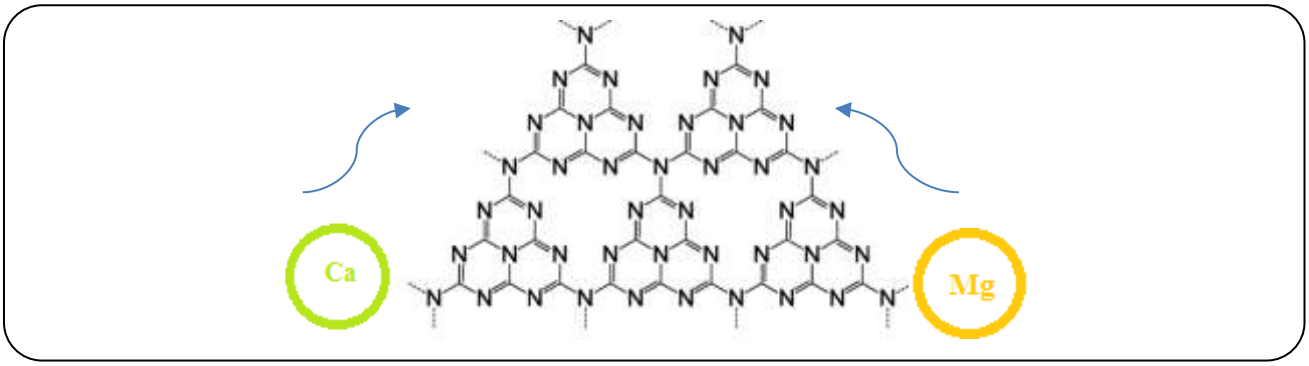

Fig. 1: Graphitic carbon nitride.

by a Unicam Galaxy 5000 instrument and FE-SEM instrument (Tescan-Chek). Atomic Absorption Spectroscopy (AAS) was performed by a 240 FS AA RF-5301PC Spectrofluorometer (Agilent, United States), and Wide-angle X-Ray Diffraction (XRD) measurements were carried out by a XPertPro diffractometer using Cu-Kα radiation (λ=1.54 A°). Atomic force microscopy (AFM) images were obtained using the Bruker Icon instrument (United States).

Preparation of graphitic carbon nitride nanosheet

The direct pyrolysis of melamine produced the bulk g-C_3N_4 [27,34]. First, melamine was heated at 580 °C for 2 h to produce a yellow powder, then the product was ultrasounded for 5 h and subsequently centrifugated to obtain g-C_3N_4 nanosheet.

Adsorption tests

Batch tests were carried out to select the optimum conditions including pH, the amounts of ions and g-C_3N_4 nanosheet, equilibrium time, and temperature. The g-C_3N_4 nanosheet (0.01-0.1 g) was added to a backer containing 25 ml of Ca^{2+} and Mg^{2+} ions (5-30 mg/L) at pH range of 2-9, under the temperature of 15-45 ℃ for 0-120 min. All samples were centrifuged and subsequently analyzed using Atomic Absorption Spectroscopy (AAS). In addition, to minimize the error, the point of zero charges (PZC) for g-C_3N_4 nanosheet was obtained [34].

The amounts of adsorbed calcium and magnesium ions on g-C_3N_4 nanosheet (q_{eq}) were determined using Eq. (1), and the removal efficiency (*Re*) was calculated using Equation (2):

$$q_{eq} = \frac{(C_0 - C_e)V}{M} \quad (1)$$

$$R_e = \frac{(C_0 - C_e)}{C_0} \times 100 \quad (2)$$

Where q_e (mg/g) is the amount of adsorbed calcium and magnesium ions. C_0 and C_e are the initial and equilibrium concentrations of the ions (mg/L), *V* is the volume (L) and *M* is the mass (g) of the g-C_3N_4 nanosheet.

Computational methods

The Quantum Espresso package was used to obtain Density Functional Theory (DFT) calculations *via* gradient approximation (GGA) with Perdew-Burke-Ernzerhof (PBE) functional [35-37]. The tri-*s*-triazine structure (14 atoms per cell unit) was studied at 12×12×1 k-points by the Monkhorst-Pack scheme.

The g-C_3N_4 nanosheet structure was optimized, composed of 54 C and 72 N atoms. The Ca^{2+} and Mg^{2+} ions were added to g-C_3N_4 nanosheet, then the kinetic energy cutoff, K point, and electronic properties of the bare and ion-adsorbed g-C_3N_4 nanosheets were calculated and subsequently compared to each other.

The intensity of interaction between the ions and 2D g-C_3N_4 was calculated using the adsorption energy Equation (3):

$$E_{ad} = E(ion - g - C_3N_4) - E(g - C_3N_4) \quad (3)$$

E (ion-g-C_3N_4) is the energy of Ca^{2+} or Mg^{2+} ions adsorbed on g-C_3N_4 nanosheet, and *E* (ion) is the ion energy of Ca^{2+} or Mg^{2+}.

RESULTS AND DISCUSSION

Characterization of g-C_3N_4 nanosheet

FT-IR analysis

To confirm the g-C_3N_4 nanosheet structure, FT-IR technique was applied to investigate its formation (Fig. 2).

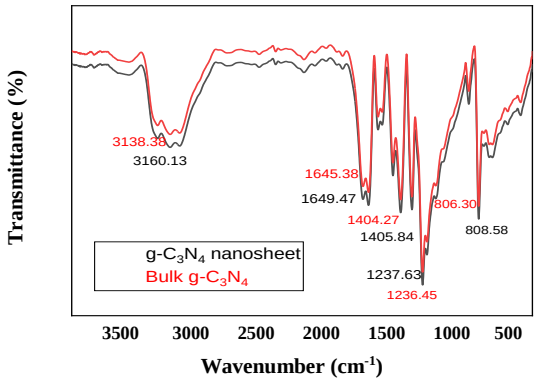

Fig.2: FT-IR spectra of bulk g-C_3N_4 and g-C_3N_4 nanosheet.

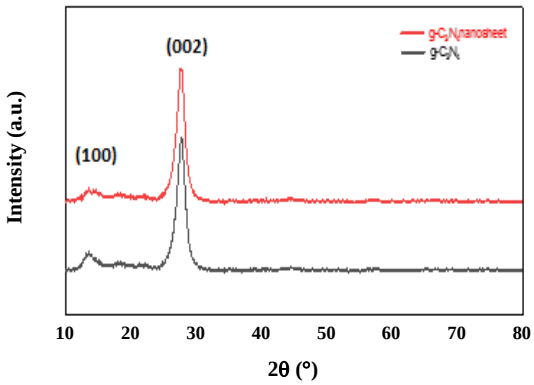

Fig. 3: XRD patterns of bulk g-C_3N_4 and g-C_3N_4 nanosheet.

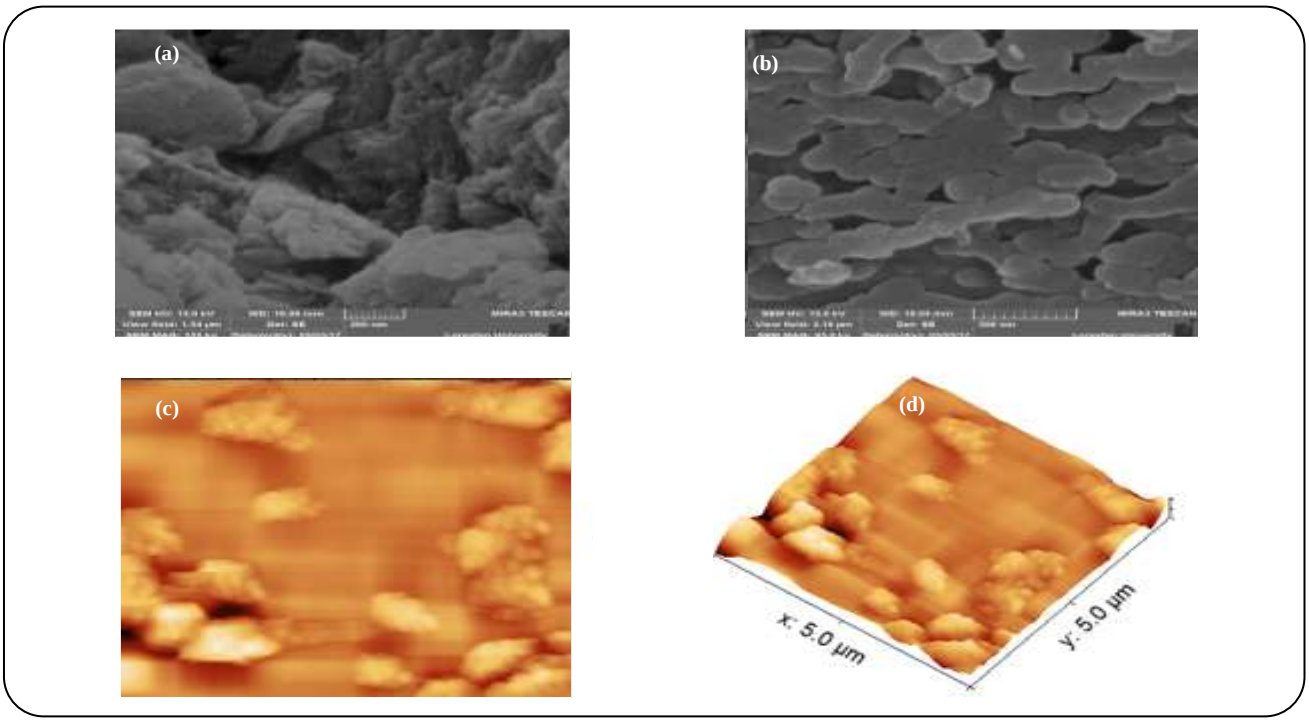

Fig. 2. SEM images of (a) bulk g-C_3N_4 and (b) g-C_3N_4 nanosheet, and (c) AFM image of g-C_3N_4 nanosheet.

Further, the FT-IR spectra of bulk/g-C_3N_4 and g-C_3N_4/ nanosheet are similar together indicating the same chemical construction. The related bands of primary and secondary amines were observed at 3000 and 3200 cm^{-1}, respectively. The formation of the C=N–C bonds was evidenced by the presence of the peaks observed at 900 ~1800 cm^{-1}. The appeared band at 808 cm^{-1} was related to the tri-*s*-triazine structure [20].

X-ray diffraction analysis

X-Ray Diffraction (XRD) pattern of g-C_3N_4 nanosheet is illustrated in Fig. 3, which represents the graphitic carbon nitride aromatic structure. The nanosheet structure of g-C_3N_4 can be evidenced by the observed decrease in the intensity of the peaks at (100) and (002) on XRD pattern of g-C_3N_4 nanosheet, compared to that of the bulk g-C_3N_4.

Morphology analysis

Fig. 4a depicts the agglomeration of bulk g-C_3N_4 at the SEM image, and the sheets of g-C_3N_4 are evidenced by Fig. 4b. Also, AFM technique was carried out to obtain the thickness of the nanosheet, the results indicated a 2 nm thickness for g-C_3N_4 nanosheet (Fig. 4c).

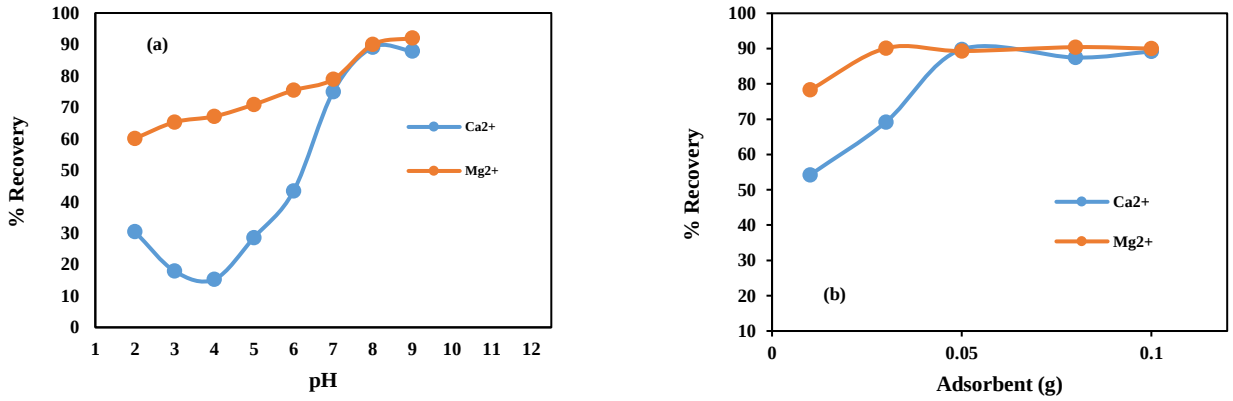

Fig. 5: Effect of (a) pH and (b) adsorbent dose for Ca^{2+} and Mg^{2+} ions adsorption on g-C_3N_4 nanosheet.

Adsorption studies

In this section, the optimization of the pH, initial concentrations of the Ca^{2+} and Mg^{2+} ions, temperature, time, and the isotherm models were investigated by adsorption on g-C_3N_4 nanosheet from aqueous solution.

pH effect

pH can play a key role in the adsorption process, because of the electrostatic interactions between ions and the surface of the adsorbent. The pH of the solution can be explained Ca^{2+} and Mg^{2+} ions uptake. The point of zero charge (PZC) related to the g-C_3N_4 nanosheet was obtained at 6.7. The optimum pH for the adsorption of Ca^{2+} and Mg^{2+} ions was achieved 8.5 and 9 in the aqueous solution, respectively. Under alkaline pHs, the g-C_3N_4 nanosheet was acquired a negative charge, whereas, under acidic conditions, it was shown a positive surface. Therefore, at a pH below PZC, the positive ions cannot be adsorbed, due to electrostatic repulsion, but at higher pHs, Ca^{2+} and Mg^{2+} ions can be adsorbed on the surface because of the strong electrostatic interaction (Fig. 5a).

Effect of the adsorbent amount

Fig. 5b represents the results of using different g-C_3N_4 nanosheet adsorbent amounts. Initially, an upwards trend was observed for the adsorption of the ions by increasing the amount of adsorbent, due to the surface area of g-C_3N_4 nanosheet was became greater, and increasing the available adsorption sites. Nevertheless, when all of the active sites were occupied, the adsorption of the ions remained constant.

Time effect

Time can be influenced the adsorption dynamics of an adsorbent, respectively. Therefore, the optimization of contact time is a critical parameter regarding the process of adsorption [38], so the contact time was optimized for adsorption of the calcium and magnesium ions on graphitic carbon nitride nanosheet under different shaking times up to 120 min. The optimum recoveries % for Ca^{2+} and Mg^{2+} ions were achieved after 90 and 60 min, especially (Fig. 6a). At the beginning of adsorption, the amount of the alkaline earth metal ion removal was high, because of the greater available surface area of the adsorbent. Upon saturation of the external sites, the rate of transportation to the internal sites became a determinant factor, until attaining equilibrium [39-41]. Therefore, it was observed that ion removal was increased up to 90 and 60 min, for Ca^{2+} and Mg^{2+} respectively, and no further increase was noted afterward.

Initial ion concentrations

Experiments were carried out to determine the most appropriate dosage of calcium and magnesium ions within the range of 5-30 mg/L. Optimum amounts of Ca^{2+} and Mg^{2+} ions were achieved at 10 and 15 ppm, respectively (Fig. 6b).

Temperature effect

The role of temperature was evaluated for the adsorption of Ca^{2+} and Mg^{2+} ions on g-C_3N_4 nanosheet within the range of 25–45 °C. The recoveries of ions were enhanced by increasing temperature, due to the mobility of ions was increased. Thus the interaction between g-C_3N_4

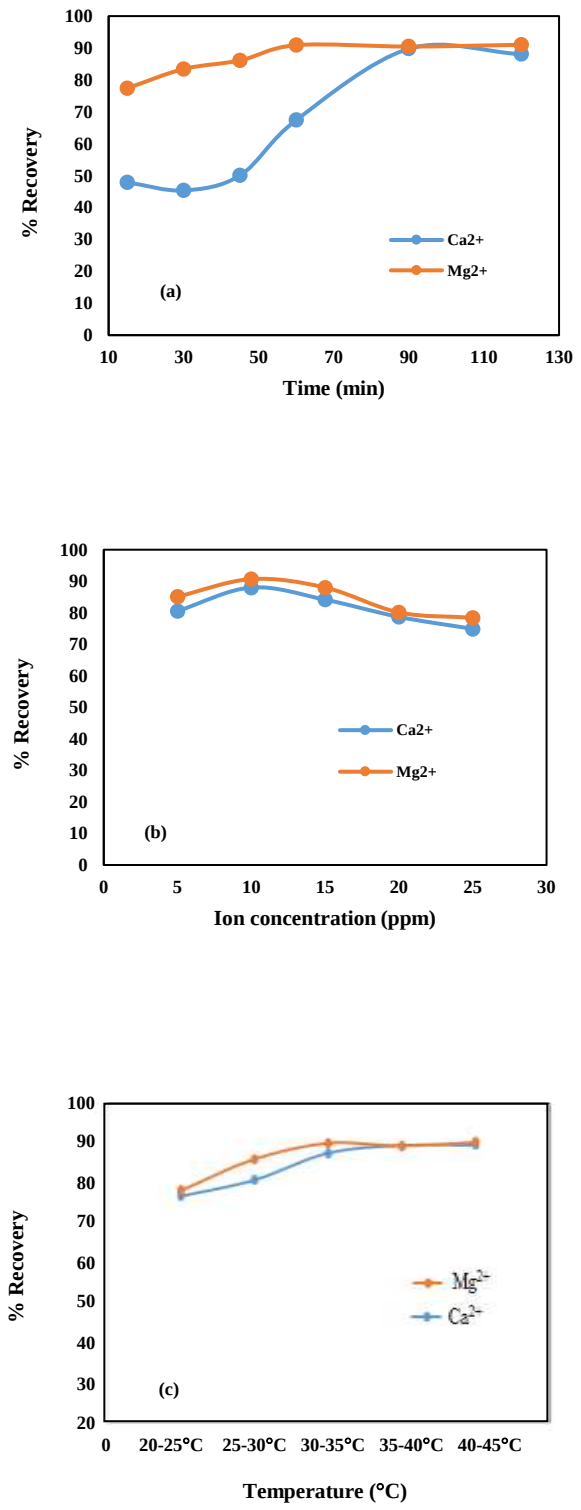

Fig. 6: Effect of (a) time, (b) ion concentrations, and (c) temperature for Ca^{2+} and Mg^{2+} ions adsorption on g-C_3N_4 nanosheet.

nanosheet and ions were improved, and the solubility of g-C_3N_4 nanosheet was changed. The experiments determined the appropriate temperature for the adsorption of calcium and magnesium ions. Finally, the optimum temperature was achieved at 32.5° C for both ions (Fig. 6c).

Adsorption Isotherm

The adsorption isotherm is an important subject for designing a suitable system [20]. In the present work, the Freundlich and Langmuir isotherms were selected to study suitable models for the adsorption of Ca^{2+} and Mg^{2+} ions on g-C_3N_4 nanosheet (Fig. 7). The Langmuir model isotherm is fitted for monolayer adsorption systems [42], and the Langmuir constant can be determined the maximum adsorption capacity per unit of the adsorbent, representing solute affinity to the adsorbent. On the other hand, the Freundlich adsorption model is assumed to be a multi-layer adsorption procedure, in which the adsorbed amount of adsorbate per unit adsorbent can be raised gradually [41]. The Freundlich and Langmuir Equations (4, 5) can be written as [41-42]:

$$\ln q_e = \ln K_f + \frac{1}{n}\ln C_e \quad (4)$$

$$\frac{C_e}{q_e} = \frac{1}{q_m b} + \frac{C_e}{q_m} \quad (5)$$

C_e: the equilibrium amounts of calcium and magnesium ions (mg/L)

q_e: the adsorbent amount of calcium and magnesium ions (mg/g)

K_f and n: constants for a given adsorbate and adsorbent

q_m: the maximum adsorption capacity (mg/g)

b: the constant related to the free energy of the adsorption (L/mg).

By using the Freundlich adsorption isotherm, the heterogeneity of adsorbent surface and multilayer adsorption can be comprehended. The graph of ln q_e versus ln C_e was plotted, and the slope and intercept were obtained to determine the value of K_f and n. The Freundlich isotherm model is demonstrated regression coefficients of R^2 = 0.95 and 0.98 for Ca^{2+} and Mg^{2+} ions on g-C_3N_4 nanosheet, respectively (Table 1).

The Langmuir isotherm turned out to be a sufficient model for the adsorption of calcium and magnesium ions (R^2 = 0.99 and 0.98) on g-C_3N_4 nanosheet. According to the Langmuir isotherm, the q_{max} of g-C_3N_4 nanosheet

Table 1: Information of the isotherm models for Ca^{2+} and Mg^{2+} ions adsorption on g-C_3N_4 nanosheet.

Ions	Freundlich			Langmuir		
	K_f (mg/g)(mg/L)^2	N	R^2	q_m (mg/g)	k_l (L mg^{-1})	R^2
Ca^{2+}	0.81	1.75	0.95	23.80	1.35	0.99
Mg^{2+}	0.59	1.46	0.96	40.00	3.68	0.98

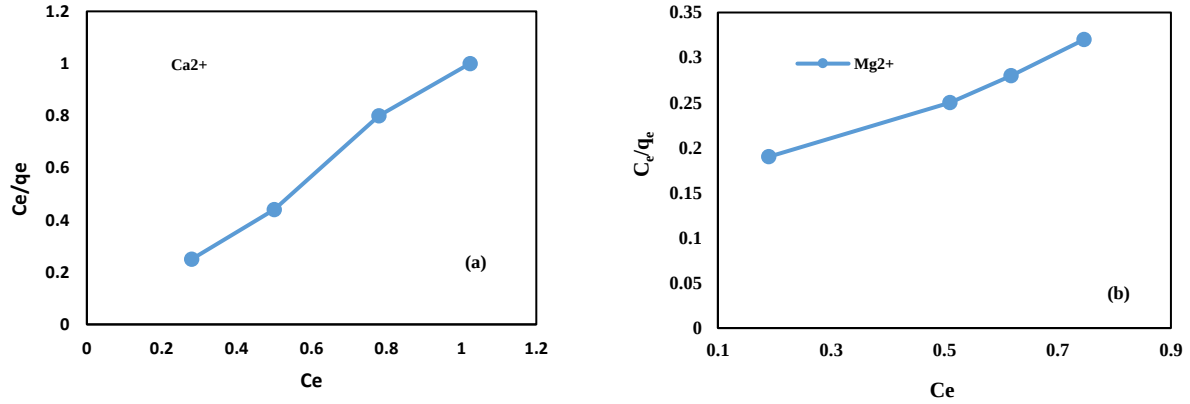

Fig. 7: Adsorption isotherms of Ca^{2+} and Mg^{2+} ions on g-C_3N_4 nanosheet by fitting Langmuir isotherm model.

for Ca^{2+} and Mg^{2+} ions were obtained by 23.80 and 40.0 mg/g.

Regeneration studies

Regeneration is a prominent factor in the selection of adsorbent. The percentages of adsorbed Ca^{2+} and Mg^{2+} ions on g-C_3N_4 nanosheet were shown to slightly change after five cycles (Mg^{2+}: 95.02%, 91.43%, 83.87%, 75.13%, and 68.63 %, and Ca^{2+}: 90.12%, 85.33%, 74.65 %, 66.10%, and 61.50 %). These findings indicated that g-C_3N_4 nanosheet can be used as a reusable and green adsorbent.

Also, the selectivity of g-C_3N_4 nanosheet was tested for Ca^{2+} and Mg^{2+} ions. The results were displayed selectivity for Ca^{2+} (Mg^{2+}>Pb^{2+}>Ni^{2+}>Co^{2+}) and Mg^{2+} (Ca^{2+}>Pb^{2+}>Ni^{2+}> Co^{2+}) ions.

Computational study

In a theoretical study, suitable geometry of g-C_3N_4 nanosheet was constructed consisting of 126 atoms (Fig. 8).

The K-point was obtained 12 Ry, and the kinetic energy cutoff was calculated between 40-400 Ry for all atoms (Fig. 9). In Figs. 10 and 11, the electronic properties of bare g-C_3N_4 nanosheets are represented including DOS, PDOS, and band structure plots. Based on the obtained results, g-C_3N_4 was shown a semi-conductive material property (E_g = 1.87 eV).

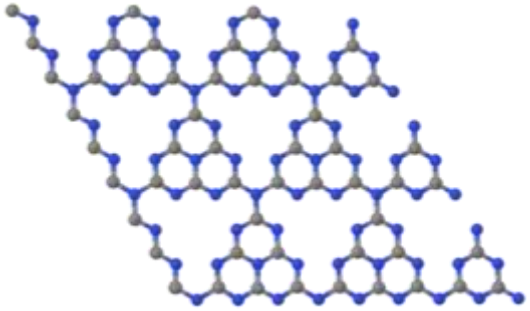

Fig. 8: Optimized structure of g-C_3N_4 nanosheet.

The different sites of g-C_3N_4 nanosheet were studied to find the stable configuration for the interaction of Ca^{2+} ions (Fig. 12). The optimum adsorption site is shown in Fig. 13, and the adsorption data related to the Ca^{2+} ion are presented in Table 2. After calculations, the best result was obtained for (b) structure, because of its more negative adsorption energy value (-15.55 eV) compared to those of other sites. This value (-15.55 eV) is much more negative than the adsorption energy previously reported for Ca^{2+} ion on penta-graphene (-2.164 eV) [9]. This result implies that the (b) structure of g-C_3N_4 nanosheet is an excellent alternative for the adsorption of these alkaline earth metal ions from aqueous solutions. The distance between Ca^{2+} and N atom was found 2.03 A^{o} on g-C_3N_4 nanosheet. In Fig. 14,

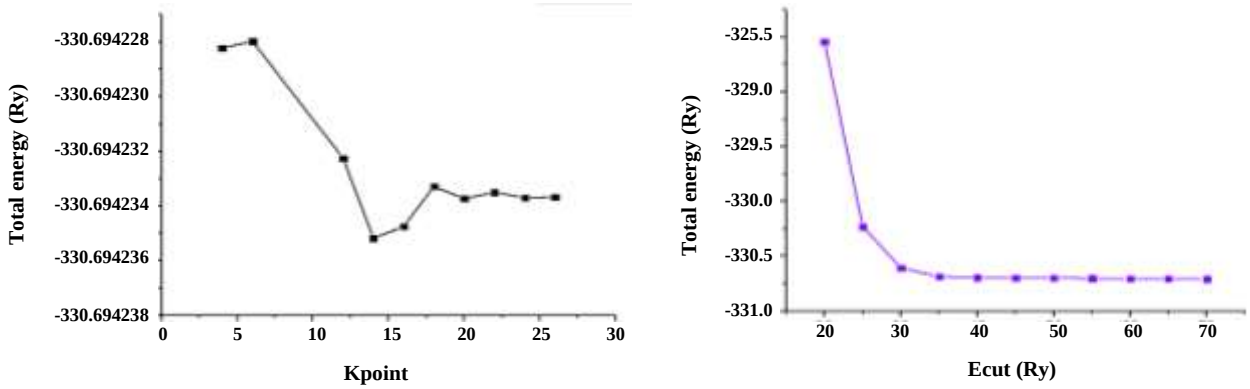

Fig. 9: The k-point and E_{cut} of g-C_3N_4 nanosheet.

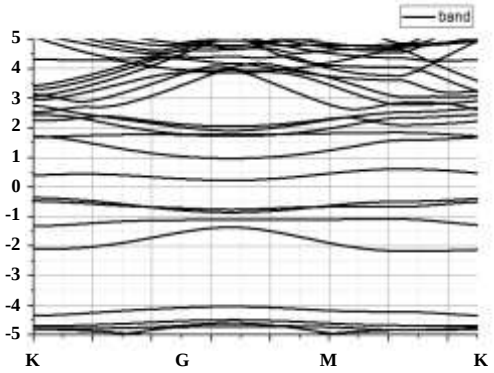

Fig. 10: Band structure diagram of g-C_3N_4 nanosheet.

the electronic properties of Ca^{2+} ion adsorption on g-C_3N_4 nanosheet are represented. The 2P layer of C and N atoms was shown to be the active site (Fig. 14 (c-d)), which Pearson's hard and soft acid-base (HSAB) principle states soft and hard acids can react with soft and hard bases [43]. The nitrogen of g-C_3N_4 nanosheet is a hard base that can be reacted with Ca^{2+} ion on g-C_3N_4 nanosheet.

Next, the interaction of Mg^{2+} ion with g-C_3N_4 nanosheet was studied to identify the stable configuration for the interaction of Mg^{2+} on 2D g-C_3N_4 structure (Fig. 15). Several configurations were examined, and the optimized structure was obtained (a) configuration because of its most negative adsorption energy value (-26.24 eV) among other sites (Fig. 16). The information related to the adsorption of Mg^{2+} ion on g-C_3N_4 nanosheet is presented in Table 3. Based on the obtained results, the magnesium is located at the center of the porous site of g-C_3N_4 nanosheet. In comparison with Ca^{2+} ion, Mg^{2+} is smaller in size, and the occupation of the (b) sites by Ca^{2+} ions (which are closer to each other compared to (a) sites occupied by Mg^{2+} ions can result in repulsive interactions among positively charged metal ions. The strong repulsion raises the electrostatic energy, resulting in slight movement of the Ca^{2+} ion away from the stable (b) site, which is unfavorable to E_{ads} (-15.55 vs. -26.24 eV). The distance between Mg^{2+} and N atom on 2D g-C_3N_4 was found to be approximately 2.77- 2.79 A°. Figs. 17 and 18 are illustrated the electronic properties of g-C_3N_4 nanosheet. DOS plots are indicated that the valence and conduct levels of the modified g-C_3N_4 nanosheet by Mg^{2+} was shown low distance and energy (-0.005 eV) compared to that of the bare g-C_3N_4 nanosheet (1.878 eV). Based on the obtained data, graphitic carbon nitride nanosheet can be converted into an intrinsic semiconductor (p-type one).

In Table. 4, the values of E_{ads}, HOMO, LUMO, and E_g for Ca^{2+} and Mg^{2+} ions on g-C_3N_4 nanosheet are represented. The adsorption of these ions on 2D g-C_3N_4 was favorable, because of the negative values of adsorption energies. One of the key factors for a favorable interaction is indicated by the energy difference between the HOMO of the nucleophile and LUMO of the electrophile. The LUMO energy of Ca^{2+} and Mg^{2+} (0.11 eV and -1.65 eV) as the electrophile ions displayed exothermic adsorption. Obtained results indicated that Ca^{2+} and Mg^{2+} ions can be reacted with N atom as a hard base. The charge transfer for the magnesium ion was higher than that of the calcium ion. Upon the adsorption of the Ca^{2+} and Mg^{2+} ions, charge transfer can result to the alkaline earth metal to carbon and the empty bands of g-C_3N_4 nanosheet, which can be moved down below the Fermi level and become stabilized. Since calcium and magnesium ions have low electronegativity

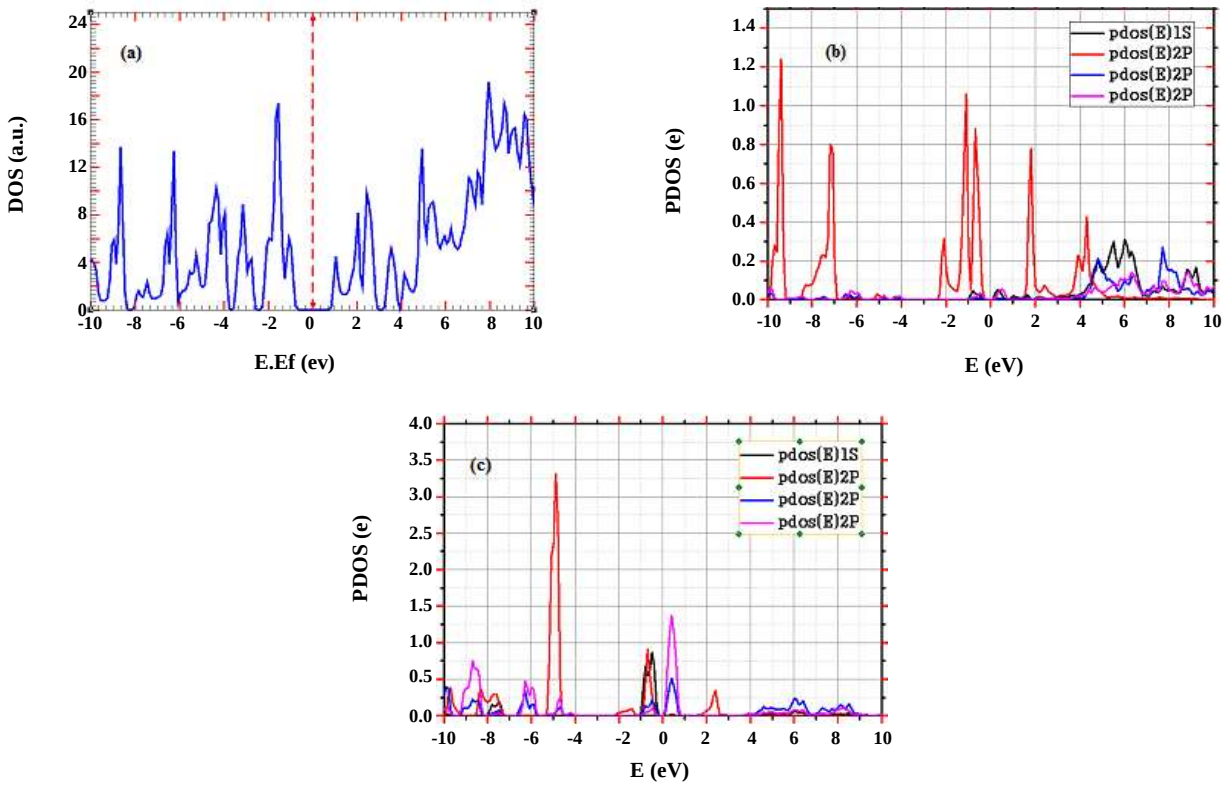

Fig. 11: Diagrams representing: a) DOS and b) PDOS of C atom, and c) PDOS of N atom in g-C_3N_4 nanosheet.

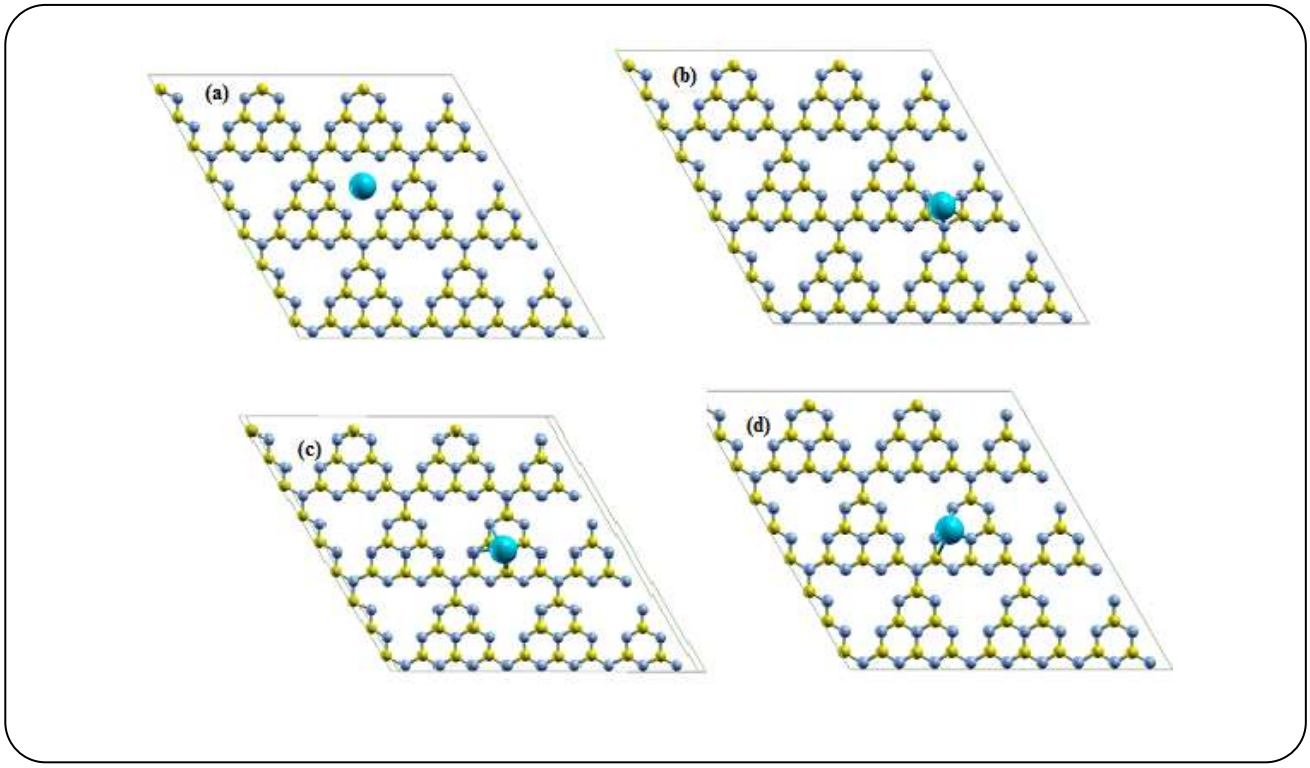

Fig. 12: Different sites of Ca^{2+} ion adsorption on g-C_3N_4 nanosheet.

Table 2: Adsorption data of Ca^{2+} ion on g-C_3N_4 nanosheet.

Entry	System	E(eV)	E_{ads} (eV)
1	Ca^{2+}	-1795.844047	-
2	g-C_3N_4 nanosheet	-40459.21308	-
3	A	-42253.16522	1.89191422
4	B	-42270.60756	-15.55041763
5	C	-42268.27440	-13.21726763
6	D	-42268.25604	-13.19891449

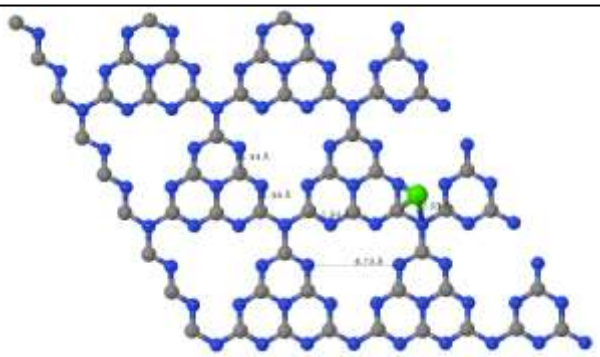

Fig. 13: Optimized structure of Ca^{2+} ion adsorbed on g-C_3N_4 nanosheet.

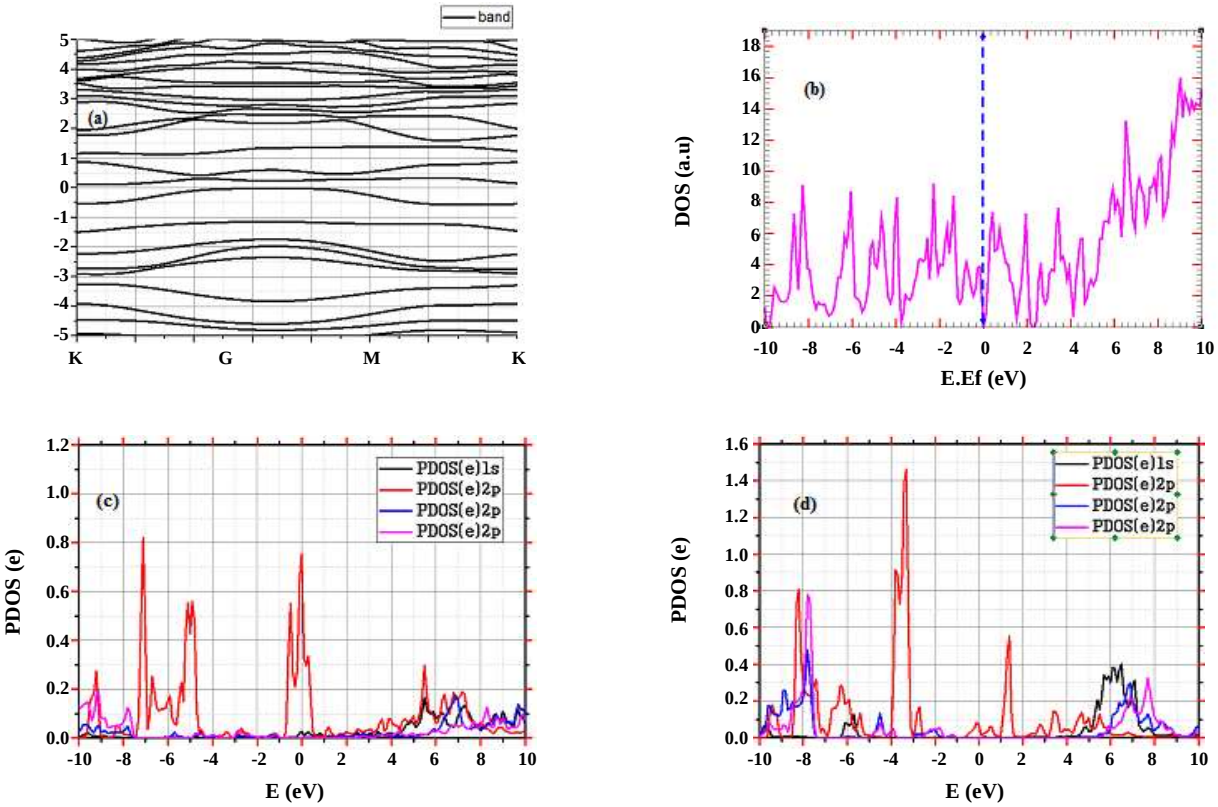

Fig. 14: Diagrams representing: a) Band structure, (b) DOS, (c) PDOS of C atom, and (d) PDOS of N atom for Ca^{2+} ion adsorbed on g-C_3N_4 nanosheet.

Table 3: Adsorption data of Mg^{2+} ion on g-C_3N_4 nanosheet.

Entry	System	E(eV)	E_{ads} (eV)
1	Mg^{2+}	-1877087956	-
2	g-C_3N_4 nanosheet	-40459.21308	-
3	a	-42363.033853	-26.2458634
4	b	-42360.43183	-23.33917581
5	c	-42336.1197	0.972959523
6	d	-42327.79333	9.299332172

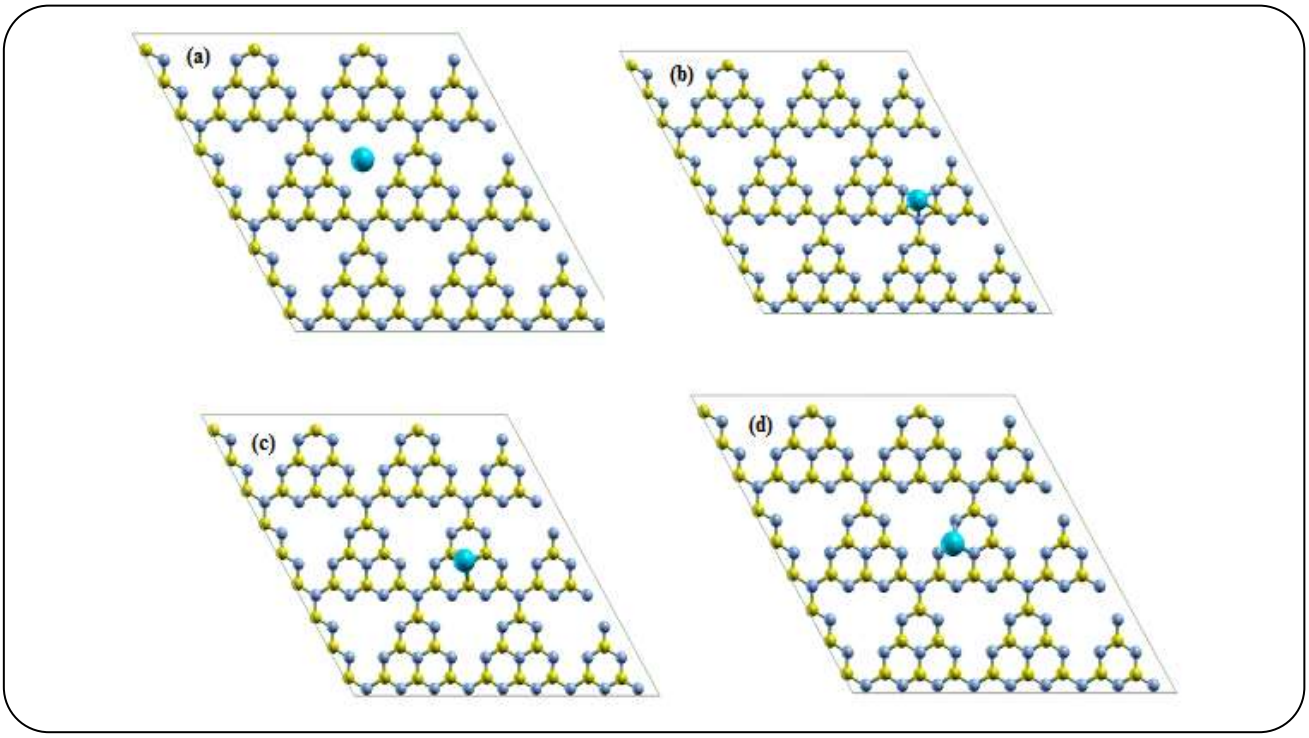

Fig. 15: Different sites of Mg^{2+} ion adsorption on g-C_3N_4 nanosheet.

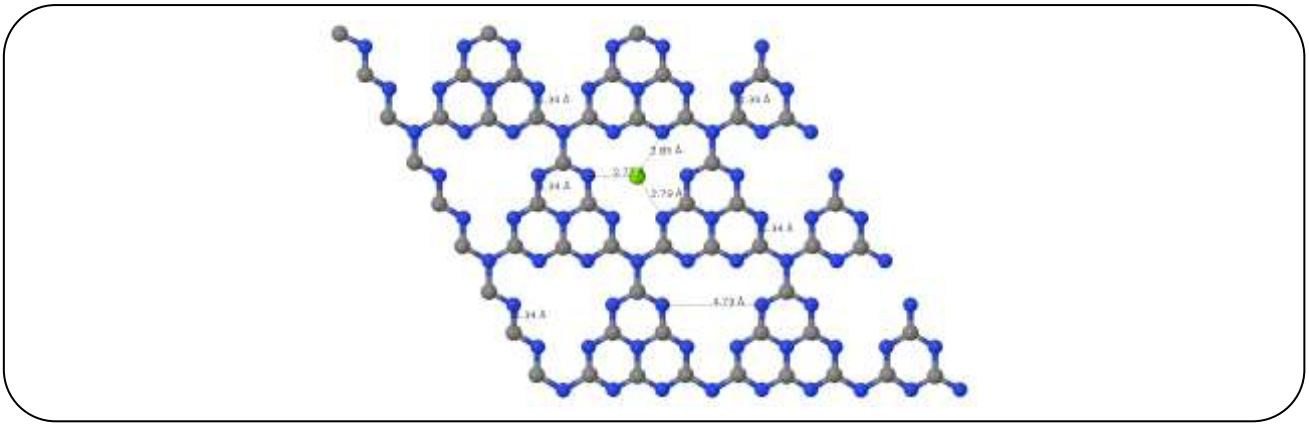

Fig. 16: Optimized structure of Mg^{2+} ion adsorption on g-C_3N_4 nanosheet.

Table 4: E_{ads}, HOMO, LUMO, and E_g of Ca^{2+} and Mg^{2+} ions adsorbed on g-C_3N_4 nanosheet.

	E_{ad} (eV)	E_{HOMO} (eV)	E_{LUMO} (eV)	E_g (eV)
g-C_3N_4	-	-4.0377	-2.15910	1.87860
Ca^{2+}	-15.5504	-0.0246	0.11790	-0.14250
Mg^{2+}	-26.24586	-1.6631	-1.65740	-0.00570

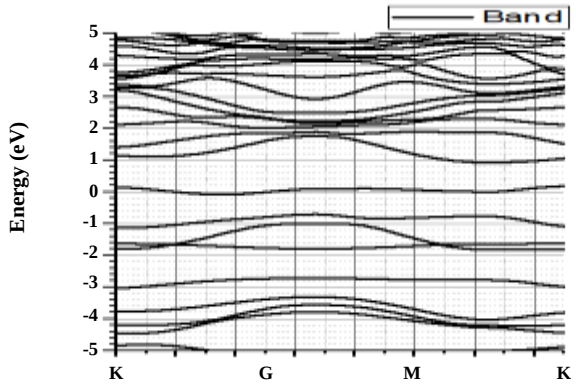

Fig. 17: Band structure of Mg^{2+} ion adsorbed on g-C_3N_4 nanosheet.

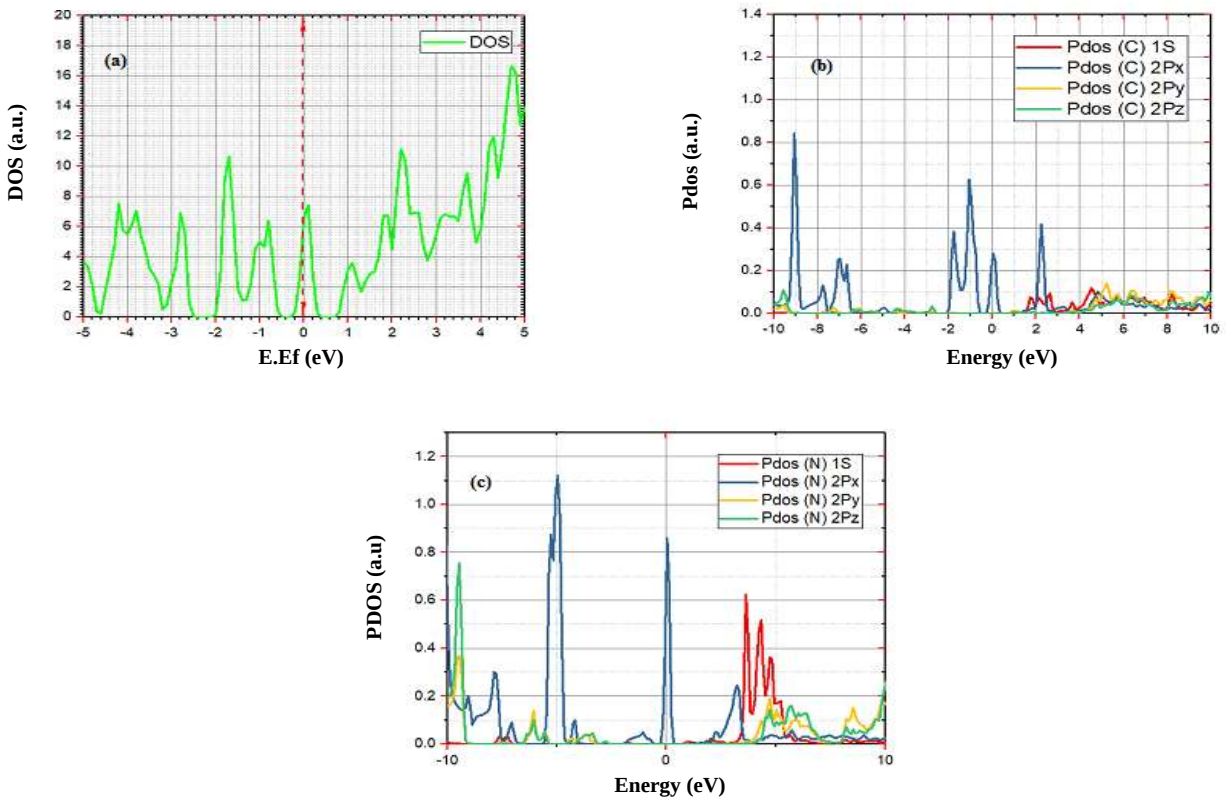

Fig. 18: Diagrams representing: (a)DOS, and (b) PDOS of C atom, and (c) PDOS of N atom for Mg^{2+} ion adsorbed on g-C_3N_4 nanosheet.

Table 5: Comparison of the results from the adsorption of Ca^{2+} and Mg^{2+} ions on g-C_3N_4 nanosheet with other compounds.

Theoretical	E_{ads} *(eV)*		
Adsorbent	Ca^{2+}	Mg^{2+}	Ref
Carbon nitride nanotube	-9.40	-11.80	[10]
H_2O	-2.47	-3.53	[44]
g-C_3N_4 nanosheet	-15.55	-26.24	The present study
Experimental	q_m (mg/g)		
Adsorbent	Ca^{2+}	Mg^{2+}	Ref.
Pistacia vera shell	2.41	2.19	[33]
Marine cyanobacterium, *gloeocapsa* species	1.00	-	[32]
g-C_3N_4 nanosheet	23.80	40.00	The present study

values, the energy obtained from the stabilized bands would be greater than that needed for charge transfer, which results in negative adsorption energies [37]. In addition, the DOS plots of Ca^{2+} and Mg^{2+} ions on g-C_3N_4 nanosheet were compared to that of the bare g-C_3N_4 nanosheet, and the results displayed a decrease in the adsorption energy of g-C_3N_4 nanosheet from 1.878 eV to -0.142 and -0.005 eV for Ca^{2+} and Mg^{2+} ions adsorbed on g-C_3N_4 nanosheet, respectively.

The findings of the present study were compared to those of the other literature (Table 5). To the best of our knowledge, no other paper concluding both the experimental and theoretical studies about the adsorption of calcium and magnesium ions were reported so far. The calculations have previously revealed that the adsorption energies of Ca^{2+} and Mg^{2+} ions on g-C_3N_4 nanosheet were higher compared to water as the solvent [44-45]. This finding can be confirmed by the efficient adsorption of Ca^{2+} and Mg^{2+} ions on g-C_3N_4 nanosheet. In theoretical studies, according to the results of *Beheshtian et al.* [10], the adsorption energies for Ca^{2+} and Mg^{2+} ions on carbon nitride nanotube were obtained -9.40 and -11.80 eV, whereas in this study, the adsorption energies were obtained -15.55 and -26.24 eV for Ca^{2+} and Mg^{2+} ions on g-C_3N_4 nanosheet, respectively. These findings imply the stronger adsorption of Ca^{2+} and Mg^{2+} ions on g-C_3N_4 nanosheet compared to carbon nitride nanotube.

In experimental studies, the g-C_3N_4 nanosheet exhibited higher adsorption capacity compared to other adsorbents. The adsorption kinetics of calcium was investigated using the marine cyanobacterium (Gloeocapsa sp.) from an aqueous solution and the influential parameters affecting the calcium removal including the initial calcium concentration, temperature, and adsorbent mass were evaluated [32]. In an assessment, *Pistacia Vera* shell was used as an adsorbent for softening hard water [33]. The obtained adsorption capacities for Ca^{2+} and Mg^{2+} ions were 2.41 and 2.19 mg/g, and it was obtained 1 mg/g by Marine cyanobacterium, *gloeocapsa* species [32-33]. Compared to these findings, the experimental results are suggested that g-C_3N_4 nanosheet is an appropriate adsorbent for the removal of the Ca^{2+} and Mg^{2+} ions from the aqueous solutions.

CONCLUSIONS

- Graphitic carbon nitride nanosheet was prepared, and its ability for the Ca^{2+} and Mg^{2+} ions adsorption was evaluated by theoretical and experimental studies.
- The maximum adsorption capacity was obtained 23.80 and 40.00 mg/g for $Ca^{2+}$and Mg^{2+} ions.
- The removal yield of Ca^{2+} and Mg^{2+} ions were achieved 90 % and 95 % from aqueous solution by g-C_3N_4 nanosheet.
- The adsorption energies of Ca^{2+} (-15.55 eV) and Mg^{2+} (-26.24 eV) ions adsorbed on g-C_3N_4 nanosheet were higher than their corresponding hydration energies (-2.47 eV and -3.53 eV).

Numencluture

AAS	Atomic Absorption Spectroscopy
AFM	Atomic Force Microscopy
Ca^{2+}	Calcium
$CaCl_2$	Calcium chloride

DFT	Density Functional Theory
DOS	Density of States
E_{ads}	Adsorption Energy
E_g	Gap Energy
FT-IR	Fourier Transform Infrared
g-C_3N_4	Graphitic carbon nitride
GGA	Gradient Approximation
HCl	Hydrochloric acid
HOMO	Highest Occupied Molecular Orbital
LUMO	Lowest Unoccupied Molecular Orbital
M	Mass
Mg^{2+}	Magnesium
$MgCl_2$	Magnesium chloride
NaOH	Sodium hydroxide
PBE	Perdew-Burke-Ernzerhof
DOS	Partial Density of States
Re	Removal efficiency
SEM	Scanning Electron Microscopy
V	Volume
XRD	X-ray Diffraction

Received : Feb. 11, 2021 ; Accepted : Jun. 14, 2021

REFERENCES

[1] Keshvardoost Chokami M., Eslami F., Zamani A., Parizanganeh A., Pir, F., Preparation of Chitosan/Iron Oxide Nanocomposite: Morphology and Study of Adsorption Characteristics for Removal of Azo-Dye from Contaminated Waters, *Iran. J. Chem. Chem. Eng. (IJCCE)*, **36**: 105-115 (2017).

[2] Parsazadeh N., Yousefi F., Ghaedi Mehrorang Karimi R., Borousan F., Optimization of Disulphine Blue Dye Adsorption Process on Zno-Cr Loaded on Activated Carbon Using Response Surface Methodology and Modeling by Means of Artificial Neural Network. *Iran. J. Chem. Chem. Eng. (IJCCE)*, **37**: 37-54 (2019).

[3] Schroeder H. A., Nason A. P., Tipton I. H., Essential Metals in Man: Magnesium, *J. Chronic. Dis. Manag.* **21**: 815-841 (1969).

[4] Graber T. W., Yee A. S., Baker F. J., Magnesium: Physiology, Clinical Disorders, and Therapy, *Ann. Emerg. Med*., **10**: 49-57 (1981).

[5] Zeppenfeld K., Electrochemical Removal of Calcium and Magnesium Ions from Aqueous Solutions, *Desalination*. **277**: 99-105 (2011).

[6] Arugula M. A., Brastad K.S., Minteer S. D., He Z., Enzyme Catalyzed Electricity-Driven Water Softening System, *Enzyme Microb. Technol*., **51**: 396-401 (2012).

[7] Galanakis C., Fountoulis G., Gekas V., Nanofiltration of Brackish Groundwater by Using a Polypiperazine Membrane, *Desalination*, **286**:277-284 (2012).

[8] Li S., A New Concept of Ultrafiltration Fouling Control: Backwashing with Low Ionic Strength Water, (2016).

[9] Wang H., Luo W., Tian Z., Ouyang C., First Principles Study of Alkali and Alkaline Earth Metal Ions Adsorption and Diffusion on Penta-Graphene, *Solid State Ionics*, **342**: 115062 (2019).

[10] Beheshtian J., Baei M.T., Bagheri Z., Peyghan A. A., First Principles Study of Alkali and Alkaline Earth Metal Ions Adsorption and Diffusion on Penta-Graphene, *Appl. Surf. Sci*., **264**: 699-706 (2013).

[11] Doroudi Z., Jalali Sarvestani M. R., Boron Nitride Nanocone as an Adsorbent and senor for Ampicillin: A Computational Study, *Chem. Rev. Lett*.**,** **3**:110-116 (2020).

[12] Jalali Sarvestani M. R., Doroudi Z., Fullerene (C20) as a Potential Sensor for Thermal and Electrochemical Detection of Amitriptyline: A DFT Study, *Chem. Lett.*, **1:** 63-68 (2020).

[13] Jalali Sarvestani M. R., Ahmadi R., Farhang Rik B., Procarbazine Adsorption on the Surface of Single Walled Carbon Nanotube: DFT Studies, *Chem. Rev. Lett.*, **3**:175-179 (2020).

[14] Shahrokhi-Shahraki R., Benally C., El-Din M. G., Par J., High Efficiency Removal of Heavy Metals Using Tire-Derived Activated Carbon Vs Commercial Activated Carbon: Insights into the Adsorption Mechanisms. *Chemosphere*. **264**:128455 (2021).

[15] Bozorgian, A., Investigation and Comparison of Experimental Data of Ethylene Dichloride Adsorption by Bagasse with Adsorption Isotherm Models, *Chem. Rev. Lett.*, **3**:79-85 (2020).

[16] Liu A. Y., Cohen M. L., Prediction of New Low Compressibility Solids, *Science*., **245**: 841-842 (1989).

[17] Kesavan G., Chen S. M., Highly Sensitive Electrochemical Sensor Based on Carbon-Rich Graphitic Carbon Nitride as an Electrocatalyst for the Detection of Diphenylamine. *Microchem. J.*, **159**:105587 (2020).

[18] Sayed E.T., Abdelkareem M.A., Alawadhi H., Elsaid K., Wilberforce T., Olabi A. G., Graphitic Carbon Nitride/Carbon Brush Composite as a Novel Anode for Yeast-Based Microbial Fuel Cells, *Energy*, **221:**119849 (2021).

[19] Xiang Q., Yu J., Jaroniec M., Graphene-Based Semiconductor Photocatalysts, *Chem. Soc. Rev.*, **41**: 782-796 (2012).

[20] Thomas A., Fischer A., Goettmann F., Antonietti M., Muller J.O., Schlogl R.J.M., Graphitic Carbon Nitride Materials: Variation of Structure and Morphology and Their Use As Metal-Free Catalysts, *J. Mater. Chem.*, **18** :4893-4908 (2008).

[21] Yong W., Xinchen W., Markus A., Polymeric Graphitic Carbon Nitride as a Heterogeneous Organocatalyst: From Photochemistry to Multipurpose Catalysis to Sustainable Chemistry, *Angew. Chem.*, **51**: 68-89 (2012).

[22] Ping N., Lili Z., Gang L., Hui- Ming C., Graphene-Like Carbon Nitride Nanosheets for Improved Photocatalytic Activities, *Adv. Func. Mater.*, **22**: 763-4770 (2012).

[23] Sun J. X., Yuan Y. P., Qiu L. G., Jiang X., Xie A. J., Shen Y. H., Zhu J. F., Fabrication of Composite Photocatalyst gC_3N_4–ZnO and Enhancement of Photocatalytic Activity Under Visible Light, *Dalton Trans.*, **41**: 6756 -6763 (2012).

[24] Li G., Wang B., Zhang J., Wang R., Liu H., Rational Construction of a direct Z-scheme g-C_3N_4/CdS Photocatalyst with Enhanced Visible Light Photocatalytic Activity and Degradation of Erythromycin and Tetracycline, *Appl. Surf. Sci.*, **478**: 1056-1064 (2019).

[25] Yang S., Zhou W., Ge C., Liu X., Fang Y., Li Z., Mesoporous Polymeric Semiconductor Materials of Graphitic-C_3N_4: General and Efficient Synthesis and their Integration with Synergistic AgBr NPs for Enhanced Photocatalytic Performances, *RSC Advances.*, **3**: 5631-5638 (2013).

[26] Nayak S., Mohapatra L., Parida K., Visible Light-Driven Novel g-C_3N_4/NiFe-LDH Composite Photocatalyst with Enhanced Photocatalytic Activity Towards Water Oxidation and Reduction Reaction, *J. Mater. Chem. A.*, **3**: 18622-18635 (2015).

[27]Chegeni M., Mousavi Z., Soleymani M., Dehdashtian S., Removal of Aspirin from Aqueous Solutions Using Graphitic Carbon Nitride Nanosheet: Theoretical And Experimental Studies, *Diam. Relat. Mate.*, **101**: 107621 (2020).

[28] Azofra L. M., MacFarlane D.R., Sun C., A DFT Study of Planar Vs. Corrugated Graphene-Like Carbon Nitride (G-C_3N_4) and its Role in the Catalytic Performance of CO_2 Conversion, *Phys. Chem. Chem. Phys.*, **18**: 18507-18514 (2016).

[29] Tian J., Liu Q., Asiri A.M., Al-Youbi A.O., Sun X., Ultrathin graphitic Carbon Nitride Nanosheet: A Highly Efficient Fluorosensor for Rapid, Ultrasensitive Detection of Cu^{2+}, *Anal. Chem.*, **85**: 5595-5599 (2013).

[30] Zhu L., You L., Wang Y., Shi Z., The Application of Graphitic Carbon Nitride for the Adsorption of Pb^{2+} Ion from Aqueous Solution, *Mater. Res. Express.*, **4**: 075606 (2017).

[31] Kerisit S., Parker S.C., Free Energy of Adsorption of Water and Metal Ions on the {101□4} Calcite Surface. *J. Am. Chem. Soc*. **126**: 10152-10161 (2004).

[32] Saravanakumar K., Venugopal G., Jayabalan Y., Kandasamy, K., Calcium Removal from Aqueous Solution by Marine Cyanobacterium, Gloeocapsa Species: Adsorption Kinetics and Equilibrium Studies, *IJPRA*, **2**:195-201 (2011).

[33] Pratomo U., Anggraeni A., Lubis R.A., Pramudya A., Farida I.N., Study of Softening Hard Water Using Pistacia Vera Shell as Adsorbent for Calcium and Magnesium Removal, *Procedia Chem.*, **16**: 400-406 (2015).

[34] Zhu X., Liu Y., Qian F., Zhou C., Zhang S., Preparation of Magnetic Porous Carbon from Waste Hydrochar by Simultaneous Activation and Magnetization for Tetracycline Removal, *J. Chen, Bioresour. Technol.*, **154**: 209-214 (2014).

[35] Giannozzi P. B., Bonini S., Calandra N., Car M., Cavazzoni R., Ceresoli C., Chiarotti D. G. L. C., Dabo M., et al. Quantum Espresso: A Modular and Opensource, *J. Phys. Condens. Matter.*, **21**: 395502 (2009).

[36] Heyd J., Scuseria G.E., Ernzerhof M., Hybrid Functionals Based on a Screened Coulomb Potential, *J. Chem. Phys.*, **118**: 8207-8215 (2003).

[37] Schmidt M.W., Baldridge K.K., Boatz J.A., Elbert S.T., Gordon M.S., Jensen J.H., Koseki S., Matsunaga N., Nguyen K.A., Su S., Windus T.L., Dupuis M., Montgomery J.A., General Atomic and Molecular Electronic Structure System, *J. Comput. Chem*., **14**:1347–1363 (1993).

[38] Srivastava V., Sharma Y., Sillanpää M., Green Synthesis of Magnesium Oxide Nanoflower and its Application for the Removal of Divalent Metallic Species from Synthetic Wastewater, *Ceram. Int*., **41**: 6702-6709 (2015).

[39] Eslami B., Ehsani Namin P., Ghasemi I., Azizi H., Karabi M., Ion Cadmium Adsorption from Aqueous Solution Using Nanocomposite Based on Chitosan/Functionalized Nano Graphene Platelet. *NSMSI*, **36**: 115-125 (2017).

[40] Shamsodin M., Fazli M., Nasiri M., Haghbeen K., Removal of Strontium (II) from Aqueous Solution by Adsorption Using Xerogel Synthesized by Teos: Kinetics and Thermodynamics Study. *Nashrieh Shimi va Mohandesi Shimi Iran (NSMSI)*, **34(4)**: 31-43 (2016).

[41] Hamidi A., Khazaeli E., Khazali F., Thermodynamics and Isotherm Studies of Adsorption of Cadmium (II) on Zinc Oxide Nanoparticle. *Nashrieh Shimi va Mohandesi Shimi Iran (NSMSI)*, **34**: 23-30 (2016).

[42] Langmuir I., The Adsorption of Gases on Plane Surfaces of Glass, Mica and Platinum, *J. Am. Chem. Soc*., **40**: 1361-1403 (1918).

[43] Datta D., On Pearson's HSAB principle, *Inorg. Chem*., **31**: 2797-2800 (1992).

[44] Pavlov M., Siegbahn P.E.M., Sandström M., Hydration of Beryllium, Magnesium, Calcium, and Zinc Ions Using Density Functional Theory, *J. Phys. Chem. A*., **102**: 219-228 (1998).

[45] Bakó I., Hutter J., Pálinkás G., Car–Parrinello Molecular Dynamics Simulation of the Hydrated Calcium Ion, *J. Chem. Phys*, **117**: 9838-9843 (2002).